

Full paper

Minimalist and multi-functional human machine interface (HMI) using a flexible wearable triboelectric patch

Qiongfeng Shi^{a,b,c,d,1}, Zixuan Zhang^{a,b,c,d,1}, Tao Chen^{e,**}, Chengkuo Lee^{a,b,c,d,f,*}

^a Department of Electrical and Computer Engineering, National University of Singapore, 4 Engineering Drive 3, Singapore, 117576, Singapore

^b Center for Intelligent Sensors and MEMS (CISM), National University of Singapore, Block E6 #05-11, 5 Engineering Drive 1, Singapore, 117608, Singapore

^c Hybrid-Integrated Flexible (Stretchable) Electronic Systems (HIFES) Program, National University of Singapore, Block E6 #05-3, 5 Engineering Drive 1, Singapore, 117608, Singapore

^d NUS Suzhou Research Institute (NUSRI), Suzhou Industrial Park, Suzhou, 215123, PR China

^e Jiangsu Provincial Key Laboratory of Advanced Robotics, School of Mechanical and Electric Engineering, Soochow University, Suzhou, 215123, PR China

^f NUS Graduate School for Integrative Science and Engineering (NGS), National University of Singapore, Singapore, 117456, Singapore

ARTICLE INFO

Keywords:

Triboelectric nanogenerator (TENG)
Human machine interface
Self-powered
Writing pad
Identification
Control interface

ABSTRACT

Human machine interfaces are of increasing importance in our daily life to connect human intentions with machine actions. Recently, triboelectric interfaces are being extensively investigated in order to achieve flexible wearable and self-powered capability simultaneously. However, drawbacks exist in current designs for the detection of common human interactions, such as large number of sensing elements and electrodes, poor output performance, and interacting experience, etc. This work presents a flexible triboelectric interacting patch with only four sensing electrodes to detect various human machine interactions. The four electrodes are configured in the layout of a splitting ring. Initially, by leveraging the individual areas and common jointing areas of the four electrodes, eight functional electrodes points are defined, which can achieve position sensing with clear differentiations even under different types of operations including both tapping and sliding interactions. Moreover, nine additional points out of the electrode areas can be defined as well for more advanced sensing of operation positions and manners, through distinguishing the unique patterns of the generated voltage. With these pre-defined points, the interacting patch can be applied as general interface for various human machine interactions. Based on the fabricated device, functional interfaces for writing trace recognition, identification code system and remote control are successfully realized, showing the high applicability of the device in diversified human machine interactions. Indicating by these affluent demonstrations, the developed interacting patch exhibits great potential in various interacting applications, e.g., writing pad, security, smart control, entertainment, virtual reality, augmented reality, and robotics, etc.

1. Introduction

In recent years, flexible and wearable sensors have received extensive development and experienced flourishing prosperity across the world, making their ways toward diverse applications in amusement, healthcare, and human machine interface [1–4]. Among these applications, human machine interfaces together with wearable electronics are of more and more importance to link up human intentions with machine actions, ranging from daily operation of electronics to

manipulation of exoskeletons for rehabilitation [5,6]. Nowadays, most of the reported flexible wearable sensors are developed based on the sensing mechanisms of resistive [7], capacitive [8], piezoelectric [9,10], triboelectric [11–13], or their hybrid mechanism [14–16]. Generally speaking, resistive and capacitive sensors require continuous power supply to achieve functional operation, which greatly increases the power consumption of the whole system. On the other hand, piezoelectric and triboelectric devices can produce self-generated electrical signals under ambient mechanical stimulus based on the

* Corresponding author. Department of Electrical and Computer Engineering, National University of Singapore, 4 Engineering Drive 3, Singapore, 117576, Singapore.

** Corresponding author. Jiangsu Provincial Key Laboratory of Advanced Robotics, School of Mechanical and Electric Engineering, Soochow University, Suzhou, 215123, PR China.

E-mail addresses: chent@suda.edu.cn (T. Chen), elelc@nus.edu.sg (C. Lee).

¹ Both authors contributed equally to this work.

<https://doi.org/10.1016/j.nanoen.2019.05.033>

Received 6 April 2019; Received in revised form 12 May 2019; Accepted 12 May 2019

Available online 21 May 2019

2211-2855/ © 2019 Published by Elsevier Ltd.

piezoelectric or triboelectric effect of the materials. Since the first invention in 2012 by Prof. Z. L. Wang and his team [17], triboelectric nanogenerator (TENG) has become one of the most popular self-powered solutions for the aforementioned applications, due to its superior advantages including diverse configurations, easy manufacturing, high performance, no material limitation and low cost [18–22]. Along these years, it has received tremendous research interests and efforts internationally for a wide range of applications, with several developing trends clearly observed from the TENG technology roadmap, e.g., water wave energy harvesting toward the blue energy dream [23–27], medical/implanted healthcare monitoring and treatment [28–30], the new era of internet of things (IoT) [31–34], advanced human machine interfaces [35–40], etc.

The integration of human machine interfaces with TENG technology enables the realization of flexible wearable and self-powered interfaces, remarkably broadening the usage adaptation and enhancing the interacting experience. Lately, various triboelectric interfaces have been developed for the applications in different areas, e.g., tactile sensor array based interfaces [41–43], novel coding interfaces [44–46], and robotic finger sensors and/or finger motion sensors [47–49], etc. In terms of human interactions upon different interfaces, tapping and sliding are two of the most commonly used operations, such as using smartphones, touch screens, writing pads, etc. In order to detect the tapping positions and sliding traces, one of the most common approaches is through multiple sensing elements forming integrated array configuration, either with separated sensing pixels and separated electrodes for each pixel [50–52], or with intersecting column and row electrodes for the entire column/row [42,53–55]. For instance, an array of 9×9 intersecting electrodes is presented for the detection of contacting position, moving trajectory and velocity when an active object is sliding on the surface [53]. Another electronic skin based interface with 5×5 electrodes is reported to monitor the planar displacement of an object above the device surface, as long as the object is pre-charged with triboelectric charges [54]. However, one main problem of the array configurations is the large number of sensing electrodes, which significantly increases the complexity in layout design, device manufacture, signal acquisition and processing.

In order to reduce the number of electrodes, devices based on the concept of analogue skin are then developed, with four electrodes located at the four edges of the sensing area [56–58]. The contact position of an object can be recognized according to the voltage ratios of the two pairs of opposite electrodes. But one drawback of this configuration is the small output performance due to the indirect coupling of triboelectric charges on the electrodes, and the associated high susceptibility of ambient noises. Moreover, only the position of each tapping can be detected using this configuration but not the sliding traces. Later on, integration of grid pattern with certain thickness on the analogue skin surface is proposed to achieve the detection of sliding traces [59]. The function of the grid pattern is to transform the continuous sliding motion into intermittent tapping motions along the sliding trace. Although such design can achieve the detection of sliding, the integration of thick grid pattern on surface introduces extra constraints to the device, largely degrading its flexibility, applicability and interacting experience. In addition, it should be noted that the small output performance and the high noise susceptibility are still not fully addressed in this design. Therefore, development of an advanced triboelectric interface with less number of electrodes and good performance is highly desirable, in order to achieve detection of both tapping and sliding interactions.

Herein, a four-electrode triboelectric interacting patch with electrodes in splitting ring configuration is proposed for various human machine interactions. By leveraging the individual areas and common jointing areas of the four electrodes, eight electrodes points are defined to detect different types of operations. Furthermore, nine additional points (one middle point and eight outer points) outside the electrode areas are defined as well for more advanced detection through pattern recognition of the generated output voltages. With these predefined

points, the device can function as general interface for various human interactions, e.g., tapping, sliding, tapping + sliding, etc. Compared to the previously reported analogue skin and non-contact based triboelectric interfaces, the developed interacting patch shows not only superior performance but also higher robustness and reliability due to the higher charge coupling efficiency. Benefited from the detection ability of different types of human operations, the developed interacting patch is then demonstrated for diversified human machine interacting applications. First, it is utilized as a writing pad for the detection of finger writing traces, which are then visually displayed on screen together with a signal acquisition and processing circuit. Then an identification code interface is developed for potential applications in door access and autonomous express delivery, through connecting each operation with one of decimal numbers or other symbols. In addition, a remote control interface is successfully demonstrated for the real-time manipulation of a wireless vehicle. With the advanced configuration design, the developed interacting patch exhibits promising potentials in various human machine interactions.

2. Design configuration and working mechanism

As illustrated in Fig. 1(a) and (b), the developed interacting patch can be conformally attached on human arm, showing great potential as flexible wearable and self-powered interface in various human machine interacting applications. The detail structure of the device is shown in Fig. 1(c), which consists of three stacking thin layers, i.e., polyethylene terephthalate (PET) substrate, patterned aluminum (Al) electrode and polytetrafluoroethylene (PTFE) friction layer. There are four sensing electrodes (labeling as E1, E2, E3 and E4 accordingly), with the layout forming a splitting ring structure. The middle main portion of each electrode forms the individual area, while the extrusion portions of two adjacent electrodes form the common jointing area. Thus there are four individual areas and four common areas around the electrode patterns, which are defined as individual electrode points and common electrode points (Point 1 – Point 8), as indicated by the black circles in Fig. 1(d). The digital photograph of the device on a flat surface is shown in Fig. 1(e), where the scale bar is 5 cm. The detail device dimensions of the interacting patch are summarized in Table S1 in the Supporting Information.

The working mechanism of the device with tapping or sliding operation on individual electrode points (Point 1, 3, 5 or 7) can be illustrated using the schematics in Fig. 1(f). Initially, all the four electrodes are connected in single-electrode triboelectric mode with resistor loads. Due to the different electron affinity of PTFE and finger (bare finger or finger wearing nitrile glove), finger surface becomes positively charged while PTFE surface becomes negatively charged after contacting with each other. In the original state, finger is staying away from the device surface. Then when finger is approaching and finally contacts the individual electrode area, electrons are driven to flow from ground to the respective electrode due to the arisen electric potential difference. Thus current flow is induced in the external circuit of that electrode, while no current flows are induced for the other three electrodes. Next, when finger leaves the device surface and back to the original position, electrons are driven to flow back to the ground, inducing an opposite current flow only on that electrode as well. In terms of the sliding operation on the individual electrode area, the working mechanism is similar to the tapping operation. When finger is sliding on the individual electrode area from other position (e.g., middle portion or outer portion of the device), current flow is induced on the respective electrode. Then when finger is sliding out of the individual electrode area, another current flow with opposite direction is generated.

Accordingly, the working mechanism with tapping or sliding operation on common electrode points (Point 2, 4, 6 or 8) can be illustrated with the schematics shown in Fig. 1(g). When finger is tapping (or sliding) on the common electrode area, the contacting area of finger can cover the extrusion portions of both electrodes. Thus the arisen

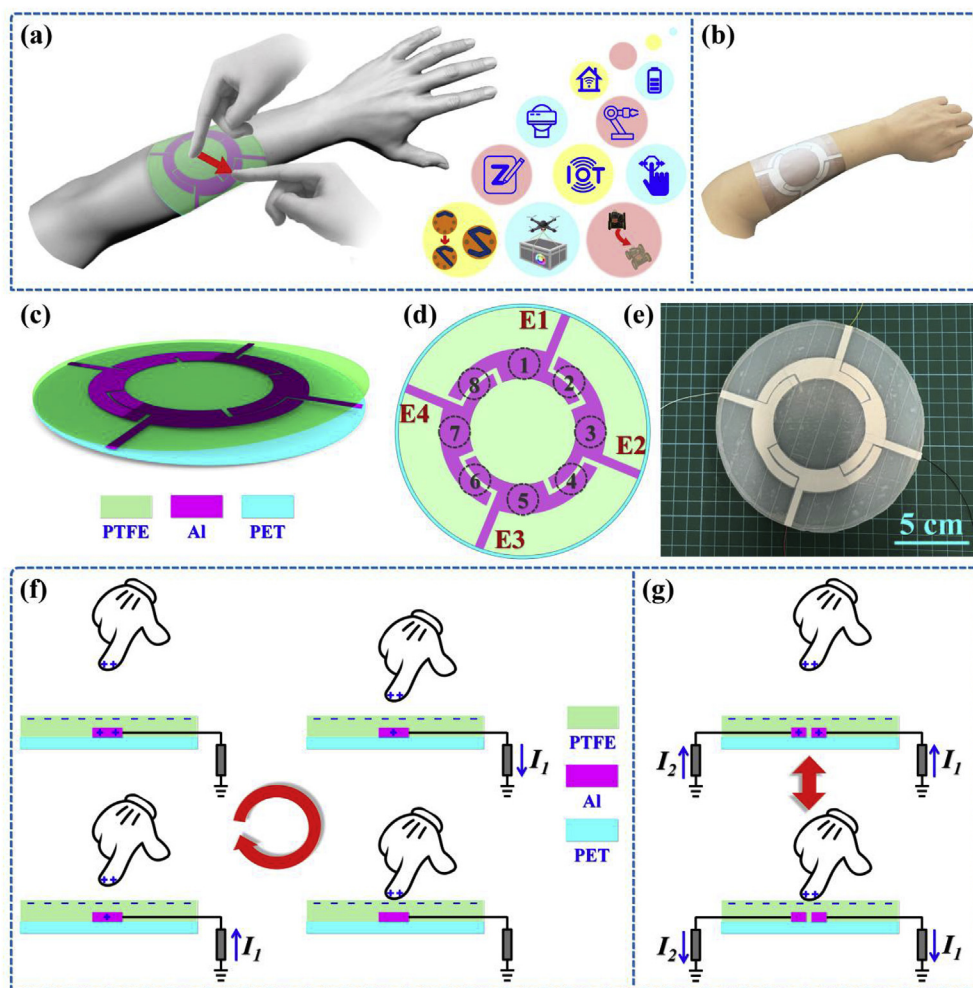


Fig. 1. Device configuration and working principle of the triboelectric interacting patch. (a) Schematic diagram of the device attached on human arm for various human machine interacting applications. (b) Digital photograph showing the flexible device can be attached conformally on arm. (c) 3D schematic diagram showing the succinct structure of the device with three thin layers. (d) Electrode layout and eight pre-defined electrode points. (e) Digital photograph of the device on a flat surface. (f) Working principle when operating on the individual electrode points (Point 1, 3, 5 and 7). (g) Working principle when operating on the common electrode points (Point 2, 4, 6 and 8).

electric potential difference induces current flows on both of the two adjacent electrodes. Later, when finger is leaving (or sliding out of) the common electrode area, current flows in the opposite direction are generated on both electrodes as well. Therefore, for tapping and sliding operations on individual electrode points, output signal is only generated on the operated electrode, while for the operations on common electrode points, output signals are generated on both of the two adjacent electrodes.

3. Characteristics with tapping and sliding interactions

According to the working mechanism of the interacting patch, when operating on individual electrode points, output signal is only generated on the corresponding electrode. When operating on common electrode points, output signals are then generated on both of the operated electrodes. For conventional triboelectric devices, their output performance is highly susceptible to the environmental and operational parameters, such as contact force, frequency, etc. One possible solution is using the voltage ratios of two or more sensing electrodes to achieve robust and reliable signal detection. Here the approach of voltage ratios is also adopted for the recognition of different operations on the device. First, the output characteristics of the device are investigated with tapping operations of different contact forces and frequencies. As illustrated in Fig. 2(a), tapping operations on Point 1, 2 and 3 are conducted and the output signals from E1 and E2 are measured. Fig. 2(d)–(f) show the output signals from Point 1, 2 and 3, respectively, with three different tapping forces (F1 ~ 0.6 N, F2 ~ 3 N, and F3 ~ 10 N) and constant frequency of ~ 1 Hz. The output voltage ratio of

V1 and V2 (i.e., V1/V2) is plotted in Fig. 2(b) for the operations of these three points. In terms of the same operated point, the absolute magnitude of output voltages increases with tapping forces, but the voltage ratio is almost not affected by tapping forces. As for different points, the output voltage ratio shows clearly noticeable variation, with the values in the range of > 10, ~ 1 and < 0.1, indicating that the voltage ratio can be used as a reliable approach for tapping position detection. Similarly, Fig. 2(g)–(i) show the output signals from Point 1, 2 and 3 with three different tapping frequencies (f1 ~ 0.75 Hz, f2 ~ 1.25 Hz, and f3 ~ 1.75 Hz) and constant tapping force of ~ 3 N. Then the output voltage ratio V1/V2 is plotted and compared in Fig. 2(c). It can also be observed that the output voltage magnitude increases with frequencies while the voltage ratio is almost not affected for the same point. The voltage ratios for different points exhibit clear difference as well, falling into the same range of > 10, ~ 1 and < 0.1. Therefore, for the tapping operations on the electrode points, the voltage ratio offers a general detection approach of different operated positions, which is highly robust against tapping force, frequency, etc.

Next, the output characteristics with different sliding operations are investigated. Fig. 3(a) illustrates the sliding operations on three electrode points (Point 1, 2 and 3), where the sliding operation starts from the middle portion of the device and across each of the three points. The output voltages when sliding on the three points are shown in Fig. 3(d)–(f), respectively, with three different sliding forces (F1 ~ 0.6 N, F2 ~ 3 N, and F3 ~ 10 N) and constant frequency of ~ 0.75 Hz. The calculated voltage ratio V1/V2 is then plotted in Fig. 3(b). It can be seen that for the same point, the magnitude of output voltages increases with sliding forces while the voltage ratio is of similar level. In terms of

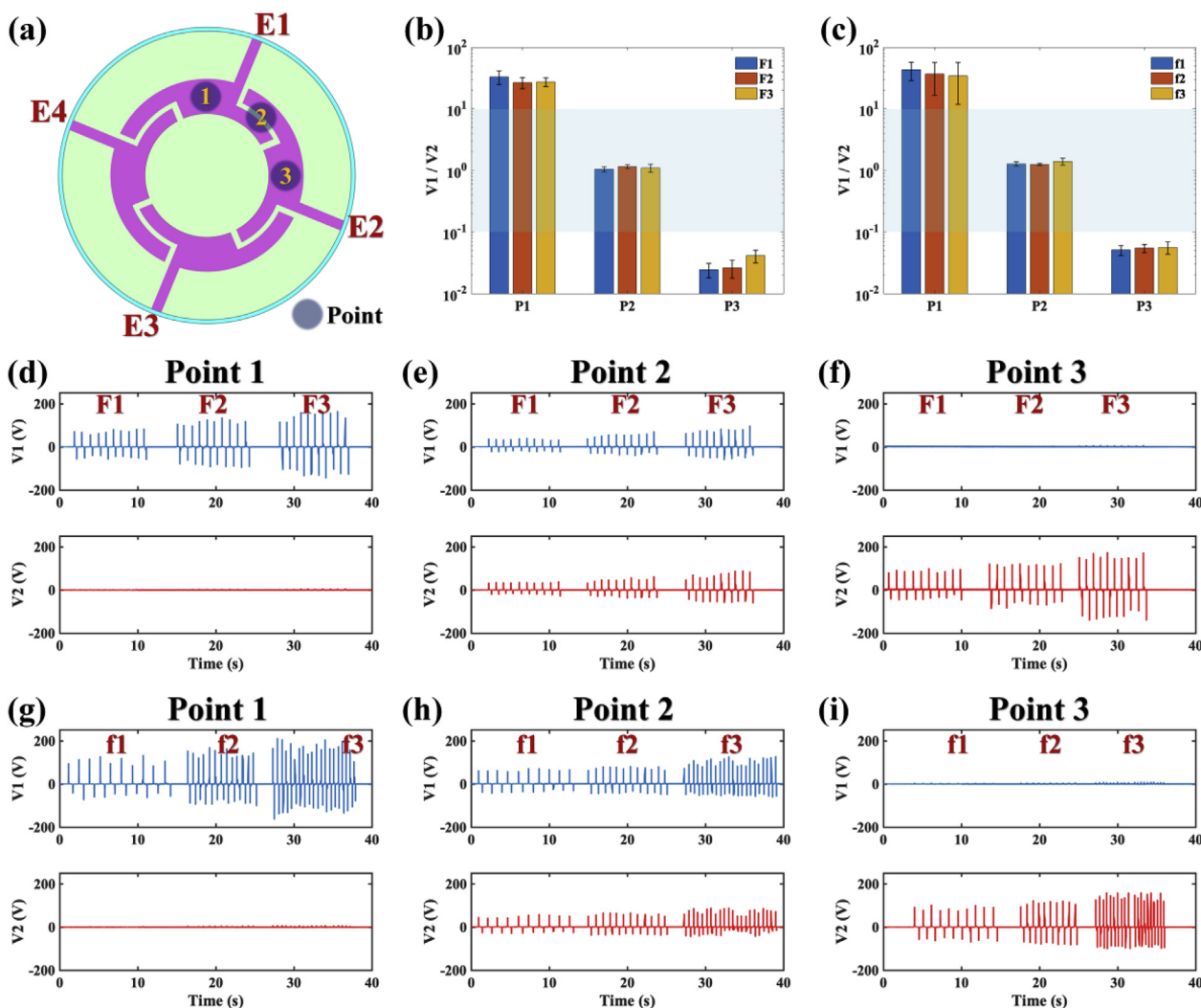


Fig. 2. Characteristics of different tapping operations. (a) Schematic diagram showing the three points under tapping. (b) Voltage ratio of V1 and V2 of the three points with different tapping forces (F1 \sim 0.6 N, F2 \sim 3 N, and F3 \sim 10 N). (c) Voltage ratio of V1 and V2 of the three points with different tapping frequencies (f1 \sim 0.75 Hz, f2 \sim 1.25 Hz, and f3 \sim 1.75 Hz). Output voltages from E1 and E2 when tapping on (d) Point 1, (e) Point 2, and (f) Point 3 with different forces. Output voltages from E1 and E2 when tapping on (g) Point 1, (h) Point 2, and (i) Point 3 with different frequencies.

different points, the voltage ratios have clearly differentiated values, in the range of > 10 , ~ 1 and < 0.1 for the three points. Then the output voltages from Point 1, 2 and 3 with three different sliding frequencies (f1 \sim 0.75 Hz, f2 \sim 1.25 Hz, and f3 \sim 1.75 Hz) and constant sliding force of ~ 3 N are shown in Fig. 3(g)–(i), respectively. The resulted voltage ratio V1/V2 is plotted in Fig. 3(c). It can also be seen that although the voltage magnitude increases with sliding frequencies, the voltage ratio is almost not affected by frequencies and follows the same trend for different points, i.e., in the range of > 10 , ~ 1 and < 0.1 . Therefore, whether it is tapping operation or sliding operation, the voltage ratio of different electrodes offers high robustness against operation force and frequency, indicating its high applicability for detection of operated positions even with different interacting manners. Besides, detail comparison of different operation manners are also performed on both individual and common electrode point, with the measurement results shown in the Supporting Information Fig. S1.

Then the characterizations of all the eight electrode points are carried out in terms of both tapping and sliding operations. Fig. 4(a) depicts the tapping positions on the eight electrode points. The generated output voltages from the four electrodes are shown in Fig. 4(b), with tapping operations performing from Point 1 to Point 8 consecutively. Then the voltage ratios of V1 against the other voltages, i.e., V1/V2, V1/V3 and V1/V4, are calculated and compared in Fig. 4(c).

The results indicate that output voltage is generated on a certain electrode only when it is tapped by finger (either the individual area or the common jointing area). Otherwise, voltage with negligible magnitude is induced on that electrode. Accordingly, the resulted values of V1/V2, V1/V3 and V1/V4 can also be categorized into the same ranges as the previous measurements (larger than 10, less than 0.1 and in between), indicating the consistency, robustness and generality of the voltage ratio based detection mechanism. In the case of Point 1 under tapping, since output voltage is only generated on E1, thus all the values of V1/V2, V1/V3 and V1/V4 are larger than 10. When Point 2 is under tapping, output voltages are then generated on both E1 and E2, leading to V1/V2 around 1 while V1/V3 and V1/V4 larger than 10. Then for Point 3, output voltage is only generated on E2, and thus V1/V2 is less than 0.1 while V1/V3 and V1/V4 are around 1. For Point 4, output voltages are only generated on E2 and E3, and thereby V1/V2 and V1/V3 are both less than 0.1 while V1/V4 is around 1. In the case of Point 5, output voltage is only generated on E3, and thus V1/V2, V1/V3 and V1/V4 are ~ 1 , < 0.1 and ~ 1 , respectively. Then for Point 6, output voltages are generated on E3 and E4, leading to V1/V2 around 1 while both V1/V3 and V1/V4 less than 0.1. Next, for Point 7, output voltage is only generated on E4, and thus both V1/V2 and V1/V3 are around 1 while V1/V4 is less than 0.1. Similarly, for Point 8, output voltages are generated on both E4 and E1, and thereby V1/V2 and V1/V3 are larger

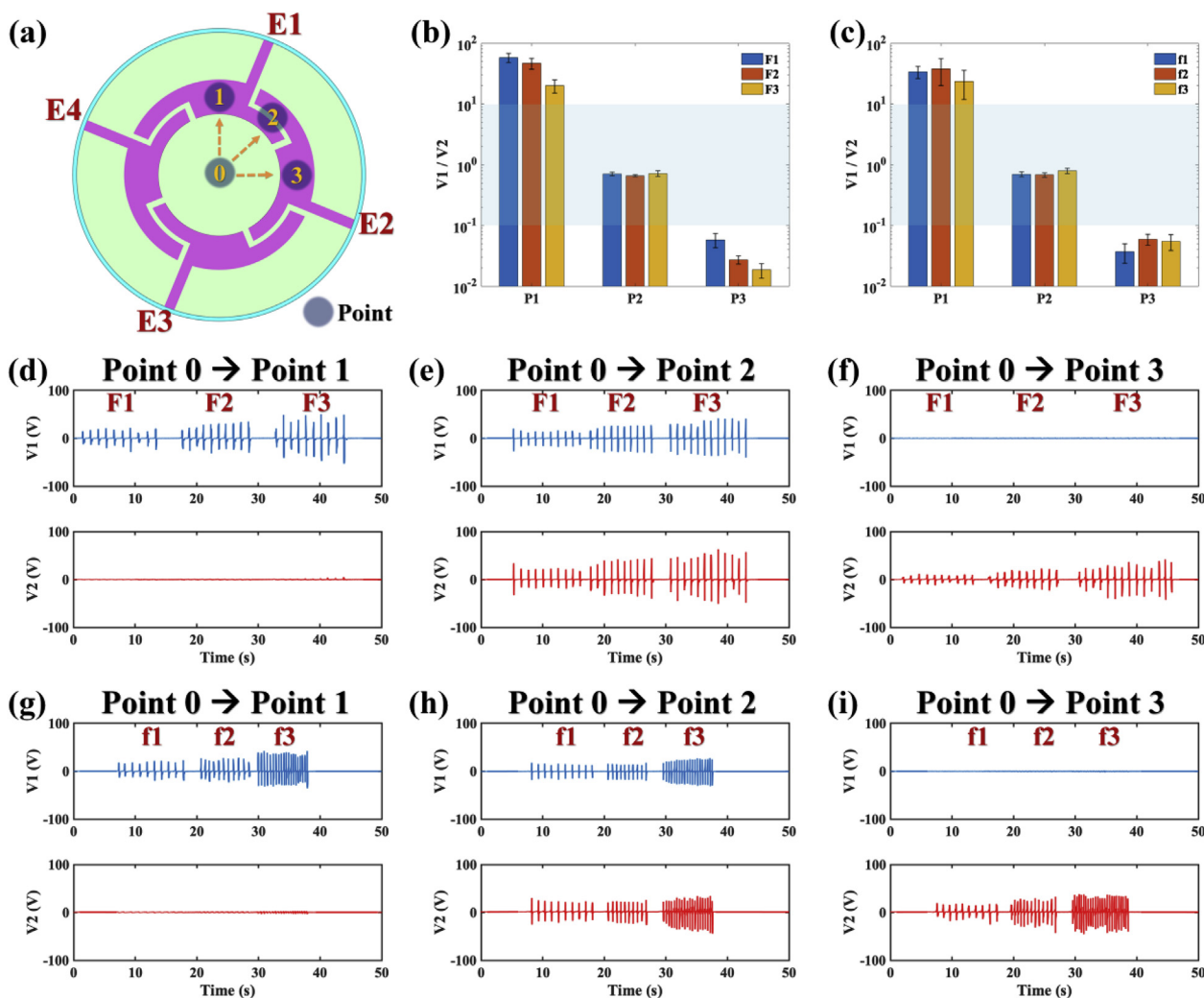


Fig. 3. Characteristics of different sliding operations. (a) Schematic diagram showing the three points under sliding. (b) Voltage ratio of V1 and V2 of the three points with different sliding forces (F1 ~ 0.6 N, F2 ~ 3 N, and F3 ~ 10 N). (c) Voltage ratio of V1 and V2 ($V1/V2$) of the three points with different sliding frequencies (f1 ~ 0.75 Hz, f2 ~ 1.25 Hz, and f3 ~ 1.75 Hz). Output voltages from E1 and E2 when repeatedly sliding on (d) Point 1, (e) Point 2, and (f) Point 3 with different forces. Output voltages from E1 and E2 when repeatedly sliding on (g) Point 1, (h) Point 2, and (i) Point 3 with different frequencies.

than 10 while $V1/V4$ is around 1. If sliding operations are performed on the eight points, similar trend of output characteristics can be observed, as shown in Fig. 4(d)–(f). Although the absolute magnitude of output voltages may change, the voltage ratios still remain consistent at the same ranges. Therefore, using voltage ratios as a general detecting mechanism, operated positions of different electrode points can be clearly distinguished under different interacting manners, offering excellent robustness and reliability in various human interactions. The ranges of the voltage ratios of all the eight electrode points from both tapping and sliding operations are summarized in Supporting Information Table S2. The output voltages after analogue-to-digital converter (ADC) are also measured and recorded, as shown in Supporting Information Fig. S2. The calculated ratios of voltage signals after ADC are consistent with previous measurements, showing that the same detection mechanism can be adopted after processing circuitry for various applications.

Benefited from the advanced electrode layout, the device can detect not only the eight electrode points defined on the electrode areas, but also additional points outside the electrode areas. As illustrated in Fig. 5(a), nine additional points outside the electrode areas are defined, i.e., middle point (M) and eight outer points on the outer side of the ring electrode (A1–A8). Human interactions on the device can be analogous to the operations of a smart phone, which normally include the

following procedures: finger contacting the device surface, sliding on the surface, ending the sliding, and leaving the device surface. Tapping can be considered as a special case with sliding distance of 0. For the particular scenarios involved the eight electrode points, the detail operation procedures can be recognized by the device. First, investigation of the output characteristics induced by operations between Point M and outer points (Point A5 and A6 as examples) are conducted, as shown in Fig. 5(a)–(c). In this case, when finger first contacts Point M, small positive peaks are also generated on all the four electrodes. Then when finger slides across Point 5 (or Point 6), successive positive and negative peaks are generated on E3 (or E3 and E4). When finger continuous slides and stops on the outer point, no output peak is generated. Then when finger leaves the device from Point A5 (or Point A6), a small negative peak is (or two small negative peaks are) generated on E3 (or E3 and E4) according to the layout of the electrodes. Similarly, output peaks with opposite polarity in a reverse order are generated from the opposite operation. The output characteristics of operations between electrode point and middle point or outer point can be found in Supporting Information Fig. S3. Basically speaking, according to the triboelectric working mechanism, when finger contacts a point outside the electrode area, only small output peak will be generated because triboelectric charges cannot be effectively coupled to the electrodes with the relatively large distance. When finger directly contacts/taps or

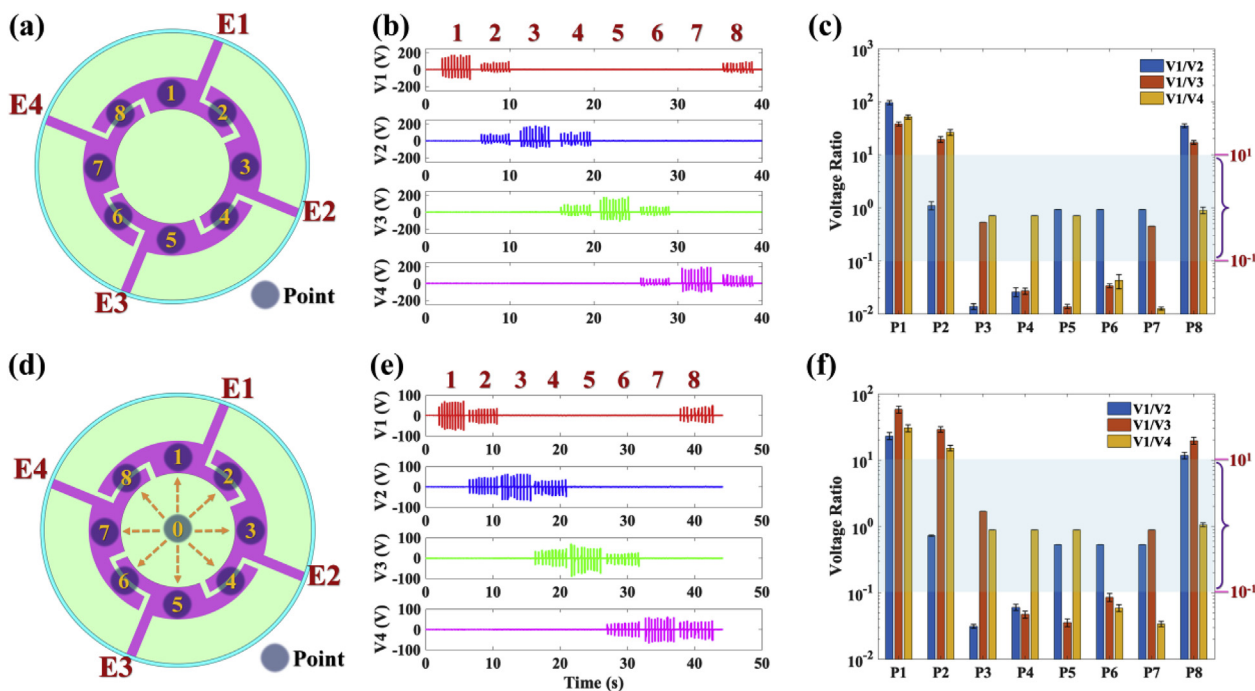


Fig. 4. Characteristics of output voltages from the eight electrode points. (a) Schematic diagram of the eight electrode points under tapping. (b) Output voltages from all the four electrodes when tapping on the eight points. (c) The corresponding output voltage ratios of V1/V2, V1/V3, and V1/V4. (d) Schematic diagram of the eight electrode points under sliding. (e) Output voltages from all the four electrodes when sliding on the eight points. (f) The corresponding output voltage ratios of V1/V2, V1/V3, and V1/V4.

slides on an electrode point, large output peak will be then generated due to effective coupling of large amount of charges on electrode. That is to say, output peaks generated from electrode points are larger than those from additional points. In terms of polarity, positive peaks are generated when finger contacts the device or slides on an electrode point, and then negative peaks are generated when finger leaves the device or slides out of an electrode point. Besides, output peaks generated from contacting and leaving an electrode point are normally larger than those generated from sliding on and out of an electrode point, since the operation period of touching/leaving is shorter than sliding.

Other than the operations involved one electrode point, operations involved two electrode points are also performed and investigated. For example, operations between Point A7 and A3 (and Point A6 and A2) and the corresponding output signals are illustrated in Fig. 5(d)–(f). First, when finger contacts Point A7 (or Point A6), a small positive peak is (or two small positive peaks are) generated on E4 (or E3 and E4). Then when finger slides across Point 7 (or Point 6), successive positive and negative peaks are generated on E3 (or E3 and E4). Next, when finger slides across Point 3 (or Point 2), successive positive and negative peaks are generated on E2 (or E1 and E2). Last, when finger leaves the device from Point A3 (or Point A2), a small negative peak is (or two small negative peaks are) generated on E2 (or E1 and E2). For the operation in opposite direction, output peaks with opposite polarity and reverse order are generated accordingly. Similarly, different output patterns can also be detected by the device with the operations between an outer point and an electrode point (across another electrode point) or between two electrode points, which can then be used to differentiate different operations as indicated in Supporting Information Fig. S4.

Except for the operations in straight lines, operations circling around the electrode points (involved multiple electrode points) are investigated as well. As illustrated in Fig. 5(g) and (h), when finger first contact Point 1, large positive peak is generated on E1. Then small negative peak is generated from E1 and small positive peak is generated from E4 for sliding to Point 8, due to the decrement of contact area for

E1 and the increment of contact area for E4. Next, small negative peak is generated from E1 and small positive peak is generated from E4 for sliding to Point 7. Last, large negative peak is generated on E4 for leaving the device from Point 7. In terms of entire-cycle circling operation starting from Point 1 as shown in Fig. 5(i), large positive peak and large negative are always generated for contacting and leaving the electrode point. For the circling operation across a certain electrode, two small positive peaks are first generated for sliding in that electrode and then two small negative peaks are generated for sliding out of that electrode. Accordingly, similar phenomenon can be observed for operations starting from common electrode point, as indicated in Supporting Information Fig. S5. Based on the above characteristics, the developed device is able to recognize various human interactions, including tapping, sliding, tapping + sliding, etc. This outstanding detection capability of the device enables itself to be adopted in wide range of advanced sensing and control applications.

4. Writing pad interface

Generally, writing is difficult to be detected by the non-pixel interfaces due to the inclusion of both tapping and sliding operations. Benefited from the excellent detection capability, the developed device is able to perform writing recognition with only four electrodes. Fig. 6 shows the writing operations on the device and the latter constructed traces of a character according to the detected positions of finger. For instance, to write the character “N” as indicated in Fig. 6(a), finger first contacts Point 8, which can be detected through the positive output peaks on both E1 and E4. Then the corresponding point is highlighted on the display screen. Next, finger slides from Point 8 to Point 6, and leaves the device from there. When finger slides out of Point 8, negative peaks are generated on both E1 and E4. Then when finger slides on Point 6 and leaves the device from there, successive positive and negative peaks are generated on both E3 and E4. After detecting Point 6, a line is constructed between the current detected point (Point 6) and the previous detected point (Point 8) through programming. Later, finger contacts Point 8 again, generating positive peaks on both E1 and E4.

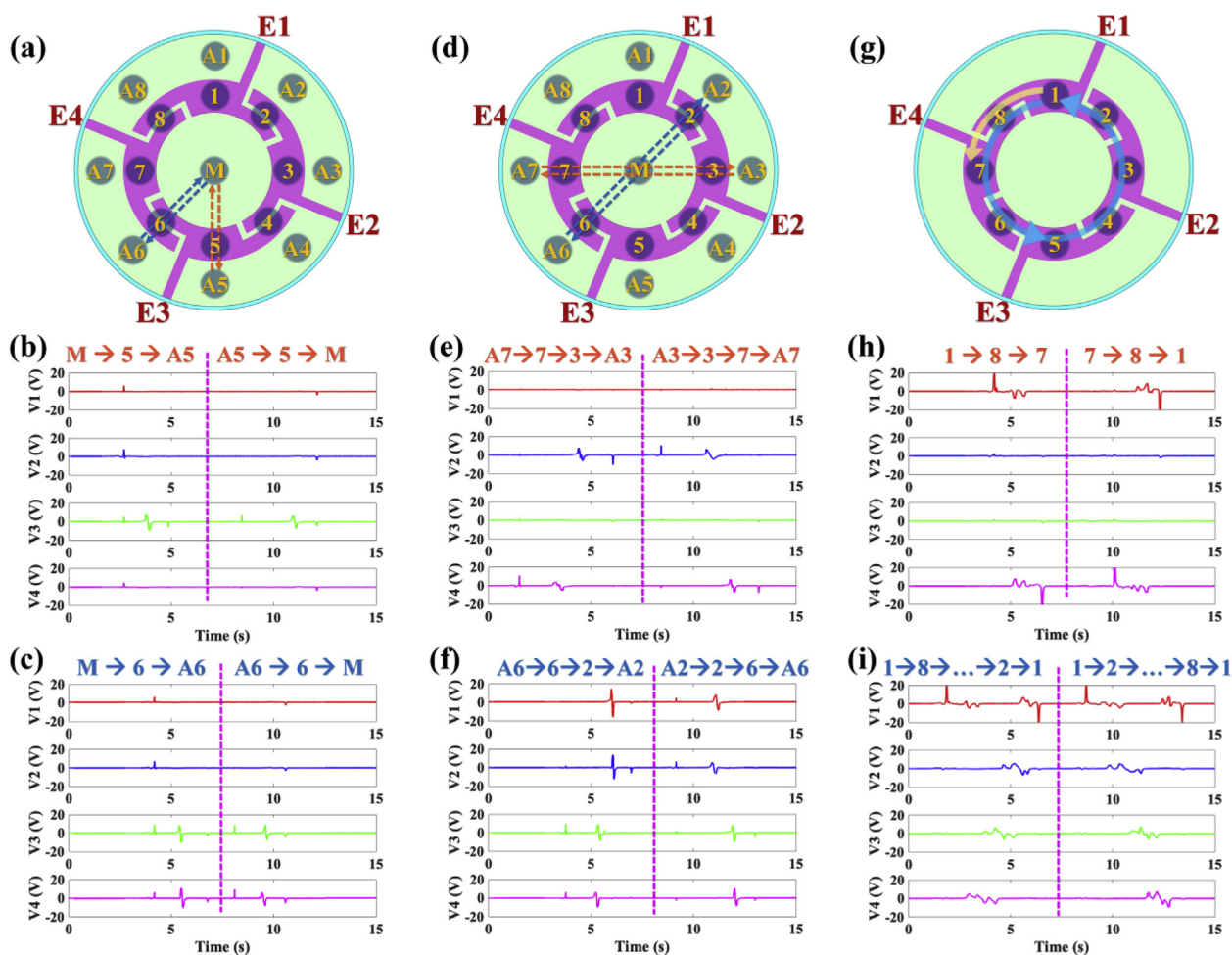


Fig. 5. Operations on the device with one or more electrode points involved (with additional eight outer points and middle point defined). (a–c) Schematic diagram and the output voltages from the operations between Point M and Point A5, and Point M and Point A6. (d–f) Schematic diagram and the output voltages from the operations between Point A7 and Point A3, and Point A6 and Point A2. (g–i) Schematic diagram and the output voltages from the operations circling the electrode points between Point 1 and Point 7, and circling around all the electrode points starting from Point 1.

After that, finger slides from Point 8 toward Point 4, generating negative peaks on both E1 and E4 first, and then positive peaks on both E2 and E3. With the detected Point 4, a line is constructed between Point 4 and Point 8. Next, finger slides from Point 4 toward Point 2 and leaves the device from there, generating negative peaks on both E2 and E3, and then consecutive positive and negative peaks on both E1 and E2. After detecting Point 2, another line is constructed between Point 2 and Point 4. Therefore, through directly writing on the device, the strokes of character “N” can be successfully constructed on the display screen according to the intuitive finger writing traces.

Similarly, for writing character “U” in Fig. 6(b), finger first taps on Point 8 and then slides sequentially on Point 6, Point 4 and Point 2, following the strokes of “U”. After the detection of Point 8, Point 6, Point 4 and Point 2 through the output peaks on the four electrodes, lines are constructed between Point 6 and Point 8, Point 4 and Point 6, and Point 2 and Point 4, respectively, forming the complete character “U” on the display screen. In the case of writing character “S” in Fig. 6(c), some traces are required to be constructed by two adjacent points. Although direct sliding between two adjacent points can be recognized through the pattern of output peaks, the magnitude is rather small which creates additional difficulty in signal detection and programming. Thus for constructing the traces between two adjacent points, individual tapping is performed on each point. In order to write the character “S”, finger sequentially taps on Point 2, Point 1 and Point 8. When finger performs the tapping on Point 8, it does not leave the

device from Point 8 but instead slides to Point 4 and leaves from there. Next, finger sequentially taps on Point 5 and Point 6 for completing the writing of “S”. Accordingly, after the detection of each of the writing points, lines are constructed between the current detected point and the previous detected point, forming the strokes of “S” on the display screen. The video showing the real-time writing of “N”, “U” and “S” can be found in Supporting Information Video S1. Through the same way, most commonly used characters and symbols can be directly written (combination of tapping and sliding) on the device, using it as an intuitive writing pad interface.

Supplementary data related to this article can be found at <https://doi.org/10.1016/j.nanoen.2019.05.033>.

5. Identification code interface

Due to the sensing capability of different operations, the interacting patch can be functionalized as the interface of identification code system, toward the potential applications such as security, door access, autonomous express delivery, etc. As illustrated in Fig. 7(a), the eight electrode points and eight outer points are defined as individual region to represent one decimal number or other functional symbol, i.e., “0” – “9”, “_”, “+”, “-”, “×”, “/”, and “=”. In addition, the sixteen points can also be defined as 4-digit binary code (“0000”, “0001”, “0010”, “0011”, “0100”, “0101”, “0110”, “0111”, “1000”, “1001”, “1010”, “1011”, “1100”, “1101”, “1110”, and “1111”) for other coding

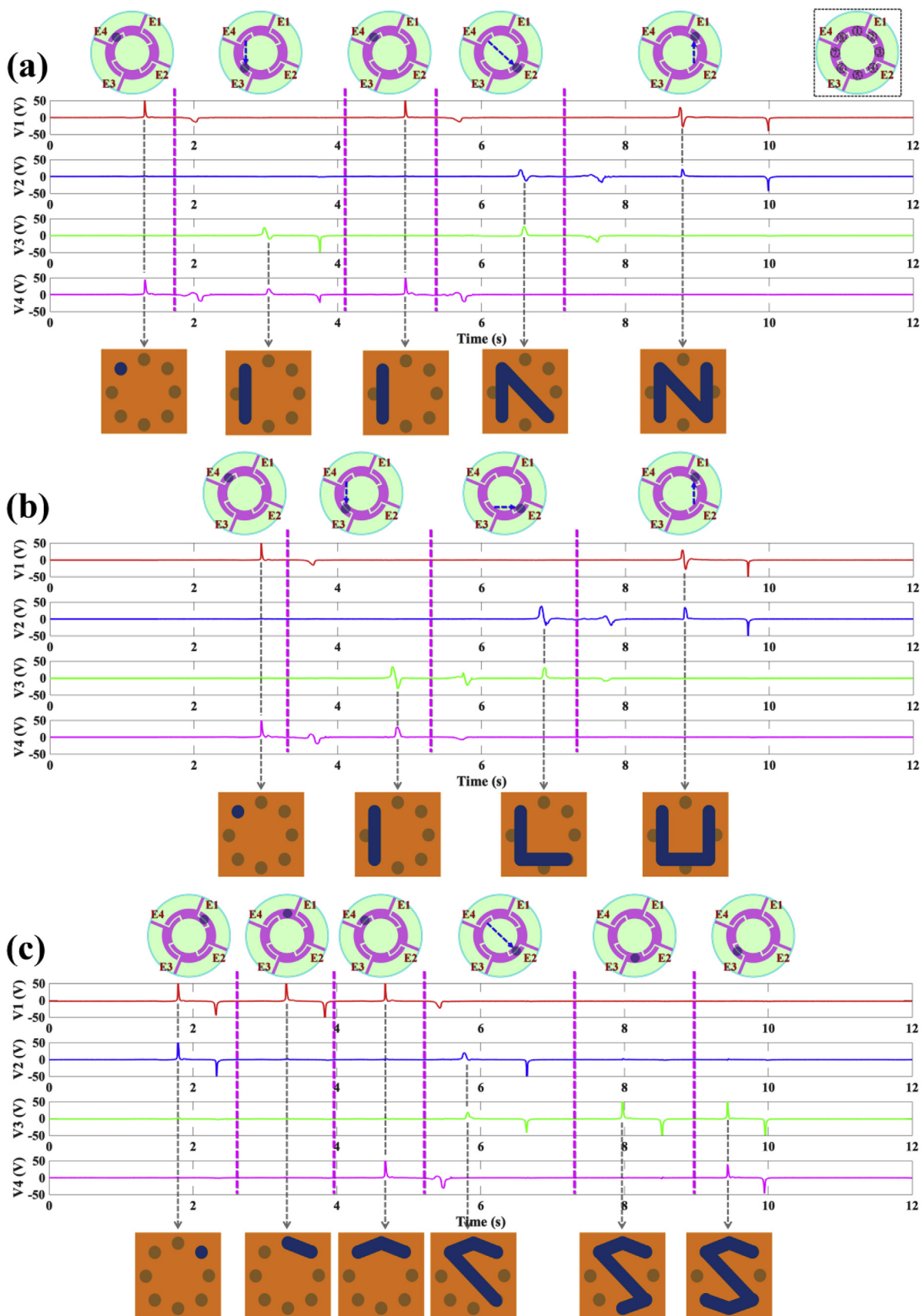


Fig. 6. Demonstration using the interacting patch as a writing interface. The detail operation procedures on the device, corresponding output voltages and the writing traces on the display screen when writing the character of (a) “N”, (b) “U”, and (c) “S”.

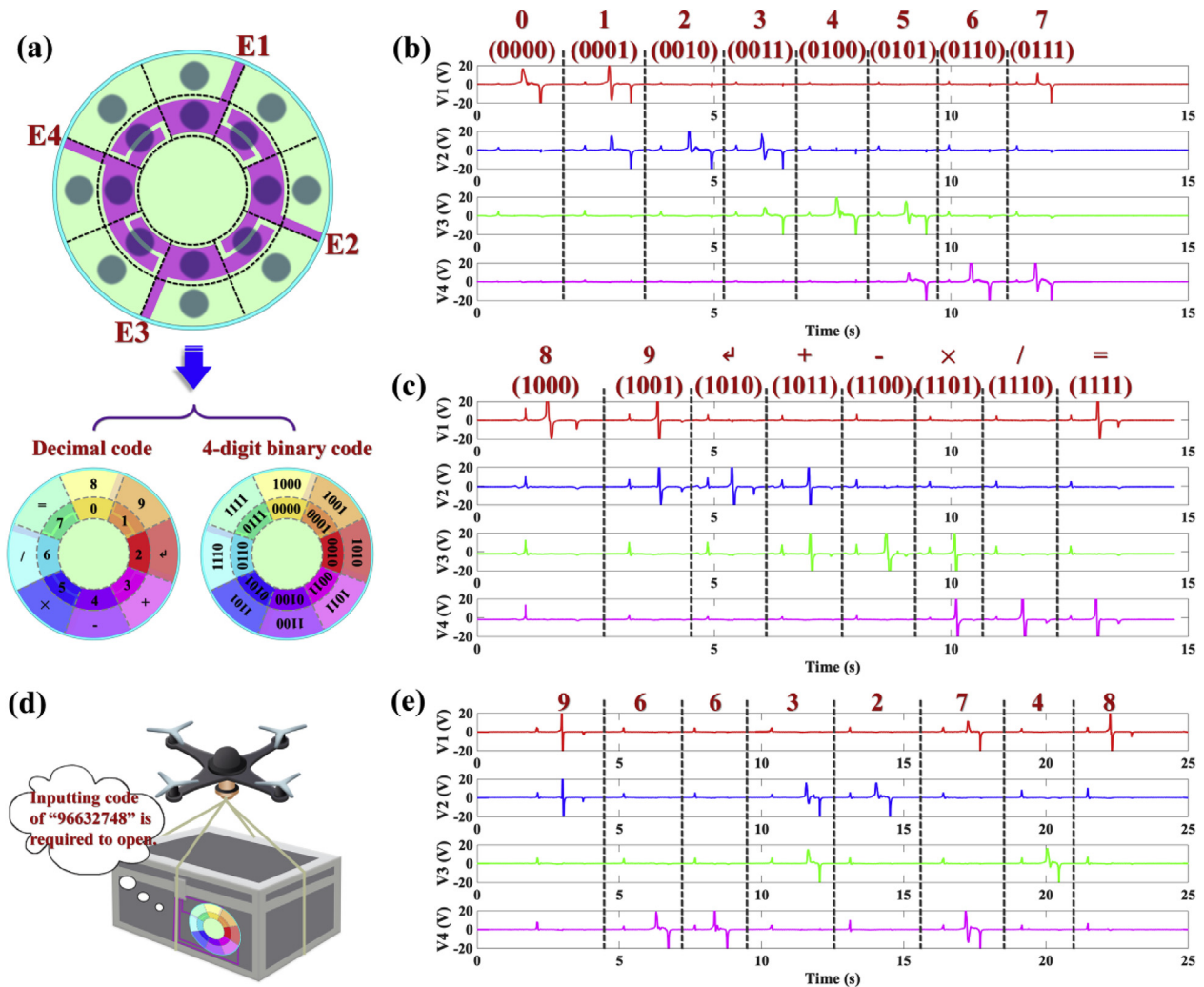


Fig. 7. Functional interface in identification code system. (a) Coding definition of the sixteen sections and the potential application scenario in autonomous express delivery. (b,c) Output voltage waveforms when finger slides on the sixteen sections. (d) A conceptual scenario of autonomous express delivery where an identification code is required to open the box for retrieving goods. (e) The output voltage waveforms of an identification code of “96632748”.

applications. To activate each number or symbol, finger is required to slide from the middle point to the predefined points and leaves the device from there. Fig. 7(b) and (c) indicate the output voltage waveforms for the respective operations on the sixteen points. For the sliding operations on individual electrode points (“0”, “2”, “4” or “6”), small positive peaks are first generated on all the four electrodes when finger contacts the middle point of the device, and then positive and negative peaks are generated on the respective electrode when finger slides on and leaves the individual electrode point. Similarly, for the sliding operations on common electrode points (“1”, “3”, “5” or “7”), small positive peaks are also generated first on all the four electrodes, and then successive positive and negative peaks are generated on both the operated electrodes forming the common electrode point. In terms of sliding to outer points (“8”, “9”, “←”, “+”, “-”, “×”, “/” or “=“), the first generation of small peaks on four electrodes is the same, while the time difference of the subsequent large positive and negative peaks is less significant since finger directly slides across the electrode point. In addition, when finger leaves the device from the outer point, small negative peak will then be generated on the respective electrode. Similarly, tapping operations can also be adopted to activate the sixteen defined sections, as shown in Supporting Information Fig. S6. Based on the generated signal patterns, activation of different points on the device can be recognized, which can be then used as the interface for inputting the identification code. A conceptual scenario of autonomous

express delivery is proposed in Fig. 7(d), where an autonomous drone is delivering the goods to buyer in a package box, with the interacting patch connecting to the electrical lock of the box. Only when the buyer inputs the correct identification code from purchase, the box will then open for the buyer to retrieve the goods. If the inputting code is incorrect, the box will remain locked to protect the goods. The generated output signals on the four electrodes for an example code (“96632748”) are shown in Fig. 7(e) to unlock the box.

6. Control interface

Other than functioning as writing pad and identification code interface, the interacting patch can also act as a control interface for gaming, entertainment, and robotics, etc. Here, using the interacting patch as the interface for wireless vehicle control is demonstrated. As depicted by the block diagram in Fig. 8(a), the complete wireless control system includes the interacting patch, signal processing circuit, microcontroller unit (MCU) module, wireless transmitter module, wireless receiver module, another MCU module, and the vehicle. First, triboelectric output signal is generated from the interacting patch when finger operates on the device. Then the output signal will go through the processing circuit before entering the MCU. The processing circuit mainly consists of several functional circuit blocks, i.e., bias circuit, amplifier circuit and low-pass filter, in order to filter out the ambient

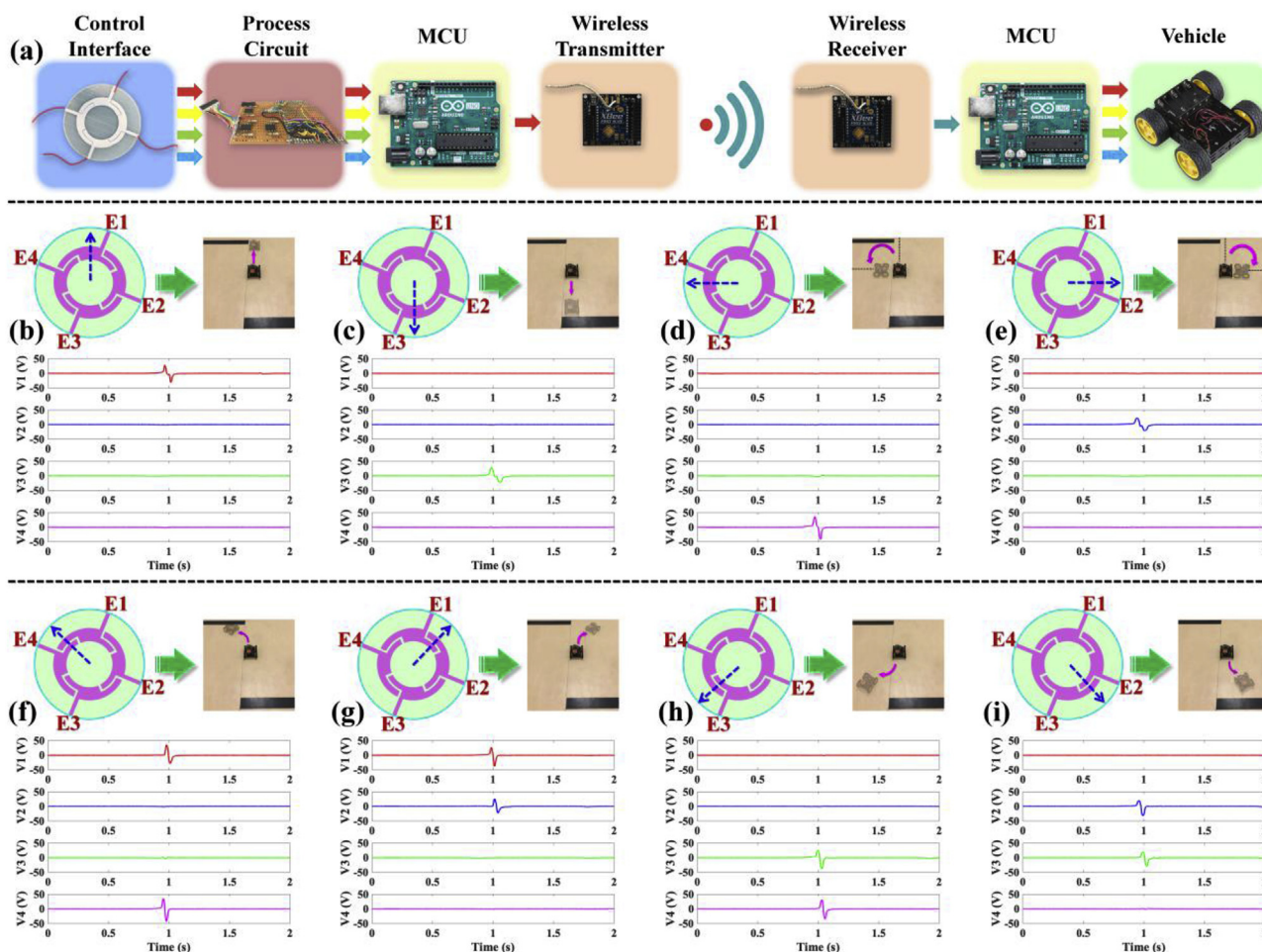


Fig. 8. Control interface for wireless vehicle manipulation. (a) Block diagram of the complete control system. Schematic diagrams of the operations, the corresponding output voltages and movements of the vehicle when controlling the vehicle to (b) go forward, (c) go backward, (d) turn left, (e) turn right, (f) go left front, (g) go right front, (h) go left rear, and (i) go right rear.

noise and remove the cross-talk between different channels, as shown in Supporting Information Fig. S7. After detecting the output signal, the MCU will perform decision making according to the pattern of the output signal. Next, the MCU will send a decision command to the transmitter module for wireless transmission. On the vehicle side, the wireless receiver module will receive the command and then send it to MCU. Based on the received command, the MCU will then generate respective control signals to drive the vehicle to perform different movements. Fig. 8(b)–(i) depict the respective control signals from the device for different movement control of a vehicle, i.e., moving forward, moving backward, turning left, turning right, going left front, going right front, going left rear and going right rear. The insets indicate the sliding operations on the device (across the eight electrode points) and the digital photographs of the corresponding vehicle movements. Sliding operations are adopted here for the vehicle control due to the higher intuitiveness of control. Similarly, the tapping operations can also be applied for the vehicle control, with the generated output signals shown in Fig. S8. The video demonstration showing real-time control of the vehicle can be found in Supporting Information Video S2.

Supplementary data related to this article can be found at <https://doi.org/10.1016/j.nanoen.2019.05.033>.

7. Conclusions

In summary, a triboelectric interacting patch is proposed with only

four sensing electrodes arranged into splitting ring structure, to distinguish the acting positions and operating manners of different human interactions, including tapping, sliding, tapping + sliding, etc. With the advanced structure design and predefined operation points, the device exhibits ultra-reliable detection and superior output performance compared to the reported analogue skin and non-contact based triboelectric interfaces. On the basis of the excellent detecting ability, various human machine interactions can be performed on the device for practical applications. Initially, the interacting patch is developed as a writing interface to capture the finger writing traces on the device for real-time display. Then interface for identification code system is developed from the device through defining different operations with appointed meanings. Besides, control interface for potential applications in gaming, virtual reality, augmented reality, entertainment and robotics, can be developed based on the device as well. Together with signal processing circuit, MCU and wireless modules, real-time demonstration of wireless vehicle control is successfully achieved. The proposed interacting patch with succinct configuration and high flexibility can be adopted as general interface in diversified human machine interacting applications.

Acknowledgement

This work was supported by: HIFES Seed Funding-2017-01 grant (R-263-501-012-133) “Hybrid Integration of Flexible Power Source and Pressure Sensors” at the National University of Singapore; Singapore-

Poland Joint Grant (R-263-000-C91-305) “Chip-Scale MEMS Micro-Spectrometer for Monitoring Harsh Industrial Gases” by Agency for Science, Technology and Research (A*STAR), Singapore and NAWA “Academic International Partnerships of Wroclaw University of Science and technology” programme by Polish National Agency for Academic Exchange Programme.

Appendix A. Supplementary data

Supplementary data related to this article can be found at <https://doi.org/10.1016/j.nanoen.2019.05.033>.

References

- [1] A. Chortos, J. Liu, Z. Bao, Pursuing prosthetic electronic skin, *Nat. Mater.* 15 (2016) 937.
- [2] X. Wang, L. Dong, H. Zhang, R. Yu, C. Pan, Z.L. Wang, Recent progress in electronic skin, *Adv. Sci.* 2 (2015) 1500169.
- [3] H. Liu, J. Zhong, C. Lee, S.-W. Lee, L. Lin, A comprehensive review on piezoelectric energy harvesting technology: materials, mechanisms, and applications, *Appl. Phys. Rev.* 5 (2018) 041306.
- [4] W. Gao, H. Ota, D. Kiriya, K. Takei, A. Javey, Flexible electronics toward wearable sensing, *Acc. Chem. Res.* 52 (2019) 523–533.
- [5] J. Wang, M.-F. Lin, S. Park, P.S. Lee, Deformable conductors for human-machine interface, *Mater. Today* 21 (2018) 508–526.
- [6] P. Kumari, L. Mathew, P. Syal, Increasing trend of wearables and multimodal interface for human activity monitoring: a review, *Biosens. Bioelectron.* 90 (2017) 298–307.
- [7] B.C.-K. Tee, A. Chortos, A. Berndt, A.K. Nguyen, A. Tom, A. McGuire, et al., A skin-inspired organic digital mechanoreceptor, *Science* 350 (2015) 313–316.
- [8] A. Atalay, V. Sanchez, O. Atalay, D.M. Vogt, F. Haufe, R.J. Wood, et al., Batch fabrication of customizable silicone-textile composite capacitive strain sensors for human motion tracking, *Adv. Mater. Technol.* 2 (2017) 1700136.
- [9] M. Wu, Y. Wang, S. Gao, R. Wang, C. Ma, Z. Tang, et al., Solution-synthesized chiral piezoelectric selenium nanowires for wearable self-powered human-integrated monitoring, *Nano Energy* 56 (2019) 693–699.
- [10] D.Y. Park, D.J. Joe, D.H. Kim, H. Park, J.H. Han, C.K. Jeong, et al., Self-powered real-time arterial pulse monitoring using ultrathin epidermal piezoelectric sensors, *Adv. Mater.* 29 (2017) 1702308.
- [11] X. He, Y. Zi, H. Yu, S.L. Zhang, J. Wang, W. Ding, et al., An ultrathin paper-based self-powered system for portable electronics and wireless human-machine interaction, *Nano Energy* 39 (2017) 328–336.
- [12] Q. He, Y. Wu, Z. Feng, C. Sun, W. Fan, Z. Zhou, et al., Triboelectric vibration sensor for a human-machine interface built on ubiquitous surfaces, *Nano Energy* 59 (2019) 689–696.
- [13] S. Lee, H. Wang, J. Wang, Q. Shi, S.-C. Yen, N.V. Thakor, et al., Battery-free neuromodulator for peripheral nerve direct stimulation, *Nano Energy* 50 (2018) 148–158.
- [14] S. Wang, Z.L. Wang, Y. Yang, A one-structure-based hybridized nanogenerator for scavenging mechanical and thermal energies by triboelectric–piezoelectric–pyroelectric effects, *Adv. Mater.* 28 (2016) 2881–2887.
- [15] M. Zhu, Q. Shi, T. He, Z. Yi, Y. Ma, B. Yang, et al., Self-powered and self-functional cotton sock using piezoelectric and triboelectric hybrid mechanism for healthcare and sports monitoring, *ACS Nano* 13 (2019) 1940–1952.
- [16] W. Yang, X. Wang, H. Li, J. Wu, Y. Hu, Z. Li, et al., Fundamental research on the effective contact area of micro-/nano-textured surface in triboelectric nanogenerator, *Nano Energy* 57 (2019) 41–47.
- [17] F.-R. Fan, Z.-Q. Tian, Z.L. Wang, Flexible triboelectric generator, *Nano Energy* 1 (2012) 328–334.
- [18] Z. Liu, H. Li, B. Shi, Y. Fan, Z.L. Wang, Z. Li, Wearable and Implantable Triboelectric Nanogenerators, *Adv. Funct. Mater.* (2019) 1808820.
- [19] S. Lee, Q. Shi, C. Lee, From flexible electronics technology in the era of IoT and artificial intelligence toward future implanted body sensor networks, *APL Mater.* 7 (2019) 031302.
- [20] H. Chen, Y. Song, X. Cheng, H. Zhang, Self-powered electronic skin based on the triboelectric generator, *Nano Energy* 56 (2019) 252–268.
- [21] Q. Zhang, Z. Zhang, Q. Liang, F. Gao, F. Yi, M. Ma, et al., Green hybrid power system based on triboelectric nanogenerator for wearable/portable electronics, *Nano Energy* 55 (2019) 151–163.
- [22] C. Wu, A.C. Wang, W. Ding, H. Guo, Z.L. Wang, Triboelectric nanogenerator: a foundation of the energy for the new era, *Adv. Energy. Mater.* 9 (2019) 1802906.
- [23] Z.L. Wang, T. Jiang, L. Xu, Toward the blue energy dream by triboelectric nanogenerator networks, *Nano Energy* 39 (2017) 9–23.
- [24] P. Cheng, H. Guo, Z. Wen, C. Zhang, X. Yin, X. Li, et al., Largely enhanced triboelectric nanogenerator for efficient harvesting of water wave energy by soft contacted structure, *Nano Energy* 57 (2019) 432–439.
- [25] J. Wang, L. Pan, H. Guo, B. Zhang, R. Zhang, Z. Wu, et al., Rational structure optimized hybrid nanogenerator for highly efficient water wave energy harvesting, *Adv. Energy. Mater.* 9 (2019) 1802892.
- [26] Q. Shi, H. Wang, H. Wu, C. Lee, Self-powered triboelectric nanogenerator buoy ball for applications ranging from environment monitoring to water wave energy farm, *Nano Energy* 40 (2017) 203–213.
- [27] X. Li, J. Tao, X. Wang, J. Zhu, C. Pan, Z.L. Wang, Networks of high performance triboelectric nanogenerators based on liquid–solid interface contact electrification for harvesting low-frequency blue energy, *Adv. Energy. Mater.* 8 (2018) 1800705.
- [28] R. Pan, W. Xuan, J. Chen, S. Dong, H. Jin, X. Wang, et al., Fully biodegradable triboelectric nanogenerators based on electrospun polylactic acid and nanostructured gelatin films, *Nano Energy* 45 (2018) 193–202.
- [29] S. Lee, H. Wang, Q. Shi, L. Dhakar, J. Wang, N.V. Thakor, et al., Development of battery-free neural interface and modulated control of tibialis anterior muscle via common peroneal nerve based on triboelectric nanogenerators (TEGs), *Nano Energy* 33 (2017) 1–11.
- [30] Z. Liu, Y. Ma, H. Ouyang, B. Shi, N. Li, D. Jiang, et al., Transcatheter self-powered ultrasensitive endocardial pressure sensor, *Adv. Funct. Mater.* 29 (2019) 1807560.
- [31] H. Ryu, J.H. Lee, U. Khan, S.S. Kwak, R. Hinchet, S.-W. Kim, Sustainable direct current powering a triboelectric nanogenerator via a novel asymmetrical design, *Energy Environ. Sci.* 11 (2018) 2057–2063.
- [32] W. Wu, X. Cao, J. Zou, Y. Ma, X. Wu, C. Sun, et al., Triboelectric nanogenerator boosts smart green tires, *Adv. Funct. Mater.* (2018) 1806331.
- [33] Y.-T. Jao, P.-K. Yang, C.-M. Chiu, Y.-J. Lin, S.-W. Chen, D. Choi, et al., A textile-based triboelectric nanogenerator with humidity-resistant output characteristic and its applications in self-powered healthcare sensors, *Nano Energy* 50 (2018) 513–520.
- [34] Q. Shi, H. Wu, H. Wang, H. Wu, C. Lee, Self-powered gyroscope ball using a triboelectric mechanism, *Adv. Energy. Mater.* 7 (2017) 1701300.
- [35] X. Pu, H. Guo, J. Chen, X. Wang, Y. Xi, C. Hu, et al., Eye motion triggered self-powered mechnosensational communication system using triboelectric nanogenerator, *Sci. Adv.* 3 (2017) e1700694.
- [36] Y.C. Lai, J. Deng, S.L. Zhang, S. Niu, H. Guo, Z.L. Wang, Single-thread-based wearable and highly stretchable triboelectric nanogenerators and their applications in cloth-based self-powered human-interactive and biomedical sensing, *Adv. Funct. Mater.* 27 (2017) 1604462.
- [37] T. Chen, Q. Shi, M. Zhu, T. He, Z. Yang, H. Liu, et al., Intuitive-augmented human-machine multidimensional nano-manipulation terminal using triboelectric stretchable strip sensors based on minimalist design, *Nano Energy* 60 (2019) 440–448.
- [38] H. Guo, X. Pu, J. Chen, Y. Meng, M.-H. Yeh, G. Liu, et al., A highly sensitive, self-powered triboelectric auditory sensor for social robotics and hearing aids, *Sci. Robots.* 3 (2018) eaat2516.
- [39] C. Wu, W. Ding, R. Liu, J. Wang, A.C. Wang, J. Wang, et al., Keystroke dynamics enabled authentication and identification using triboelectric nanogenerator array, *Mater. Today* 21 (2018) 216–222.
- [40] W. Ding, A.C. Wang, C. Wu, H. Guo, Z.L. Wang, Human-machine interfacing enabled by triboelectric nanogenerators and tribotronics, *Adv. Mater. Technol.* 4 (2019) 1800487.
- [41] J. Tao, R. Bao, X. Wang, Y. Peng, J. Li, S. Fu, et al., Self-powered tactile sensor array systems based on the triboelectric effect, *Adv. Funct. Mater.* (2018) 1806379.
- [42] X. Wang, H. Zhang, L. Dong, X. Han, W. Du, J. Zhai, et al., Self-powered high-resolution and pressure-sensitive triboelectric sensor matrix for real-time tactile mapping, *Adv. Mater.* 28 (2016) 2896–2903.
- [43] X. Pu, M. Liu, X. Chen, J. Sun, C. Du, Y. Zhang, et al., Ultrastretchable, transparent triboelectric nanogenerator as electronic skin for biomechanical energy harvesting and tactile sensing, *Sci. Adv.* 3 (2017) e1700015.
- [44] J. Chen, X. Pu, H. Guo, Q. Tang, L. Feng, X. Wang, et al., A self-powered 2D barcode recognition system based on sliding mode triboelectric nanogenerator for personal identification, *Nano Energy* 43 (2018) 253–258.
- [45] Z. Yuan, X. Du, N. Li, Y. Yin, R. Cao, X. Zhang, et al., Triboelectric-based transparent secret code, *Adv. Sci.* 5 (2018) 1700881.
- [46] Q. Shi, C. Qiu, T. He, F. Wu, M. Zhu, J.A. Dziuban, et al., Triboelectric single-electrode-output control interface using patterned grid electrode, *Nano Energy* 60 (2019) 545–556.
- [47] X. Pu, H. Guo, Q. Tang, J. Chen, L. Feng, G. Liu, et al., Rotation sensing and gesture control of a robot joint via triboelectric quantization sensor, *Nano Energy* 54 (2018) 453–460.
- [48] T. He, Q. Shi, H. Wang, F. Wen, T. Chen, J. Ouyang, et al., Beyond energy harvesting-multi-functional triboelectric nanosensors on a textile, *Nano Energy* 57 (2019) 338–352.
- [49] Q. Shi, H. Wang, T. Wang, C. Lee, Self-powered liquid triboelectric microfluidic sensor for pressure sensing and finger motion monitoring applications, *Nano Energy* 30 (2016) 450–459.
- [50] S. Li, W. Peng, J. Wang, L. Lin, Y. Zi, G. Zhang, et al., All-elastomer-based triboelectric nanogenerator as a keyboard cover to harvest typing energy, *ACS Nano* 10 (2016) 7973–7981.
- [51] Q. Shi, T. Wang, T. Kobayashi, C. Lee, Investigation of geometric design in piezoelectric microelectromechanical systems diaphragms for ultrasonic energy harvesting, *Appl. Phys. Lett.* 108 (2016) 193902.
- [52] J. Chen, P. Ding, R. Pan, W. Xuan, D. Guo, Z. Ye, et al., Self-powered transparent glass-based single electrode triboelectric motion tracking sensor array, *Nano Energy* 34 (2017) 442–448.
- [53] C.B. Han, C. Zhang, X.H. Li, L. Zhang, T. Zhou, W. Hu, et al., Self-powered velocity and trajectory tracking sensor array made of planar triboelectric nanogenerator pixels, *Nano Energy* 9 (2014) 325–333.
- [54] H. Guo, H. Wu, Y. Song, L. Miao, X. Chen, H. Chen, et al., Self-powered digital-analog hybrid electronic skin for noncontact displacement sensing, *Nano Energy* 58 (2019) 121–129.
- [55] X. Wang, Y. Zhang, X. Zhang, Z. Huo, X. Li, M. Que, et al., A highly stretchable transparent self-powered triboelectric tactile sensor with metallized nanofibers for wearable electronics, *Adv. Mater.* 30 (2018) 1706738.

- [56] M. Shi, J. Zhang, H. Chen, M. Han, S.A. Shankaregowda, Z. Su, et al., Self-powered analogue smart skin, *ACS Nano* 10 (2016) 4083–4091.
- [57] T. Li, J. Zou, F. Xing, M. Zhang, X. Cao, N. Wang, et al., From dual-mode triboelectric nanogenerator to smart tactile sensor: a multiplexing design, *ACS Nano* 11 (2017) 3950–3956.
- [58] T. Chen, Q. Shi, K. Li, Z. Yang, H. Liu, L. Sun, et al., Investigation of position sensing and energy harvesting of a flexible triboelectric touch pad, *Nanomaterials* 8 (2018) 613.
- [59] H. Feng, C. Zhao, P. Tan, R. Liu, X. Chen, Z. Li, Nanogenerator for biomedical applications, *Adv. Healthc. Mater.* 7 (2018) 1701298.



Qiongfeng Shi received his B.Eng. degree from the Department of Electronic Engineering and Information Science, University of Science and Technology of China (USTC) in 2012, and received his Ph.D. degree from the Department of Electrical and Computer Engineering, National University of Singapore (NUS) in 2018. He is currently a Research Fellow in the Department of Electrical and Computer Engineering, National University of Singapore. His research interests include energy harvesters, triboelectric nanogenerators, self-powered sensors, and wearable/implantable electronics.



Zixuan Zhang received his B.Eng. degree from the School of Mechanical and Electrical Engineering at the University of Electronic Science and Technology of China (UESTC), Chengdu, China, in 2018. He is now a Master student in the Department of Electrical and Computer Engineering, National University of Singapore. His research interests include self-powered wearable sensors, energy harvesters and triboelectric nanogenerator.



Tao Chen received the B.Sc. degree in Mechanical Design, Manufacturing and Automation, M.Sc. degree in Mechatronic Engineering, and Ph.D. degree in Mechatronic Engineering from Harbin Institute of Technology, Harbin, China, in 2004, 2006, and 2010, respectively. He is a visiting scholar in National University of Singapore in 2018. He is currently an associate professor at Soochow University, Suzhou, China. His main research interests include MEMS, sensors, and actuators.



Chengkuo Lee received his Ph.D. degree in Precision engineering from The University of Tokyo in 1996. Currently, he is the director of Center for Intelligent Sensors and MEMS, and an Associate Professor in the Department of Electrical and Computer Engineering, National University of Singapore, Singapore. In 2001, he cofounded Asia Pacific Microsystems, Inc., where he was the Vice President. From 2006 to 2009, he was a Senior Member of the Technical Staff at the Institute of Microelectronics, A-STAR, Singapore. He has contributed to more than 300 international conference papers and extended abstracts and 290 peer-reviewed international journal articles.